Nanoscale

ROYAL SOCIETY OF CHEMISTRY

PAPER

View Article Online
View Journal | View Issue

Check for updates

Cite this: *Nanoscale*, 2021, **13**, 8555

An electrically switchable anti-ferroelectric bilayer In_2Se_3 based opto-spintronic device†

Yaqing Yang,[a,b] Liwen Zhang,[a,b] Jun Chen,[c,b] Xiaohong Zheng, *[a,d] Lei Zhang, *[a,b] Liantuan Xiao[a,b] and Suotang Jia[a,b]

Received 19th January 2021,
Accepted 6th April 2021

DOI: 10.1039/d1nr00369k

rsc.li/nanoscale

Based on non-equilibrium Green's function combined with density functional theory (NEGF-DFT), we theoretically investigate the spin-related photogalvanic effect (PGE) in two anti-ferroelectric bilayer In_2Se_3 structures by atomic first-principles calculations. It is found that, due to the absence of inversion symmetry and the presence of strong spin–orbital interaction (SOI) in anti-ferroelectric bilayer In_2Se_3, the photoinduced charge-to-spin conversion can be achieved *via* the PGE. The generated spin-dependent photocurrent is largely spin-polarized and the corresponding spin polarization can vary from 0% to 100% depending on the photon energies, polarization and incident angles. Furthermore, it is found that, by tuning the polarization and the incident angles of light, the fully spin-polarized and pure spin photocurrent can be obtained. Most importantly, the spin dependent photocurrent can be largely tuned through the transition between two anti-ferroelectric bilayer In_2Se_3 states by the gate voltage. The defined relative spin dependent photoresponse change ratio n_s between two states is extremely large and its maximum value can be in the order of $\sim 10^4$. Therefore, our work demonstrates the great potential of bilayer In_2Se_3's novel application in two-dimensional non-volatile opto-spintronic devices.

1. Introduction

Ferroelectric materials attract growing research attention due to their spontaneous electric polarization.[1–3] More importantly, the corresponding two ferroelectric states of the materials can be switched by an external electric field, which is not only fundamentally interesting but also important in practical applications.[4] In addition to ferroelectricity, ferroelectrics also have many other interesting properties, such as piezoelectricity, dielectricity, and pyroelectricity, and exhibit the photoelectric effect and photorefractive effect.[5–10] Based on these fantastic electrical properties, ferroelectric materials are built into a variety of electronic components with different functionalities, for example, large-capacity capacitors, diodes, ferroelectric field-effect transistors, ferroelectric tunnel junctions, non-volatile ferroelectric random-access memories *etc.*[11–17] With the continuous miniaturization of electronic devices, traditional three-dimensional (3D) ferroelectric materials like barium titanate ($BaTiO_3$) are facing huge challenges in the nanometer scale dimensions. Since the depolarization is enhanced and the long-range Coulomb coupling is further reduced as the films scale down, it is difficult to stabilize their ferroelectricity in the nanometer range.[18] Therefore, people are trying to find ultrathin materials that present robust ferroelectricity at room temperature. Besides the traditional three dimensional materials, several two-dimensional ferroelectric materials have been theoretically predicted and experimentally confirmed recently.[19–23] In 2D van der Waals materials, the intra-layer chemical bond is strong while the inter-layer interactions are weak, which provides a pathway for realizing electric polarization in the 2D limit thickness. Among them, two dimensional In_2Se_3 is a narrow bandgap semiconductor with a direct bandgap in the near infrared range. It is found that, in addition to the out-of-plane ferroelectric polarization, two dimensional In_2Se_3 also has in-plane electric polarization at room temperature.[4,14,24–26] When the out-of-plane electric polarization is reversed, the in-plane electric polarization direction will also be reversed accordingly. On the one hand, this feature ensures that few-layer and even mono-atomic layer α-In_2Se_3 can break the critical size limit existing in traditional bulk ferroelectric materials and form a stable out-of-plane electric polarization. On the other hand, it also provides a new method for the external electric field to

[a]*State Key Laboratory of Quantum Optics and Quantum Optics Devices, Institute of Laser Spectroscopy, Shanxi University, Taiyuan 030006, China. E-mail: zhanglei@sxu.edu.cn*
[b]*Collaborative Innovation Center of Extreme Optics, Shanxi University, Taiyuan 030006, China*
[c]*State Key Laboratory of Quantum Optics and Quantum Optics Devices, Institute of Theoretical Physics, Shanxi University, Taiyuan 030006, China*
[d]*Key Laboratory of Materials Physics, Institute of Solid State Physics, HFIPS, Chinese Academy of Sciences, Hefei 230031, China. E-mail: xhzheng@theory.issp.ac.cn*
†Electronic supplementary information (ESI) available. See DOI: 10.1039/D1NR00369K

regulate ferroelectricity between the ferroelectric phase and different anti-ferroelectric (AFE) phases.[15,27]

More recently, two dimensional few-layer In_2Se_3 has been made into photodetectors, which show an unexpected broad range from ultraviolet to short-wavelength infrared.[28–33] On the other hand, the spin–orbital interaction (SOI) of two-dimensional α-In_2Se_3 is quite large due to the presence of In and Se atoms.[34] Lately, many photogalvanic effects (PGE) induced spin-dependent photocurrent are proposed in systems without inversion symmetry.[35–39] Since the inversion symmetry of α-In_2Se_3 is automatically broken,[24] it will be interesting to know whether the spin dependent photocurrent can be generated *via* the PGE in α-In_2Se_3, which has not yet been explored. If possible, we try to answer the following questions: is the photocurrent spin-polarized or not? Can we obtain the pure spin photocurrent? Can the PGE induced spin dependent photocurrent be further tuned?

In this work, we demonstrate that spin-polarized and even pure spin photocurrent can be generated *via* the PGE in two anti-ferroelectric bilayer α-In_2Se_3 based nanoscale devices by using first-principles calculations. In general, the generated spin-dependent photocurrent is spin-polarized and the corresponding spin polarization can vary from 0% to 100%. By tuning the photon energies, polarization and incident angles, fully spin-polarized and pure spin photocurrent can be obtained. More importantly, the spin dependent photocurrent can be largely tuned through the transition between two anti-ferroelectric bilayer In_2Se_3 states controlled by the external gate voltage. The relative spin dependent photoresponse change ratio n_s between two anti-ferroelectric states is extremely large and its maximum value can be in the order of $\sim 10^4$, which indicates that the proposed anti-ferroelectric bilayer α-In_2Se_3 based nanoscale device has potential applications in two-dimensional non-volatile opto-spintronic devices.

2. Theoretical formalism and computational details

As shown in Fig. 1(a and b), the atomic structures of anti-ferroelectric (AFE) bilayer α-In_2Se_3 (named α_{out} and α_{in} for simplicity) with two different ferroelectric polarizations are fully relaxed by using the Vienna ab initio simulation package (VASP).[40] During the simulation, a cutoff energy of 400 eV was set for the plane wave expansion. Both structures were fully relaxed until the forces acting on each atom are less than 0.01 eV $Å^{-1}$. The optimized lattice constants along the y and x directions are 7.11 Å and 4.11 Å, respectively. The interlayer spacing d (shown in Fig. 1(b)) of the α_{out} structure and α_{in} structure is 4.51 Å and 4.54 Å, respectively. It is found that the total energy of the α_{in} structure is 1.7 meV lower than that of the α_{out} structure when SOI is included. Next, the quantum transport calculations are carried out by using the Keldysh non-equilibrium Green's function (NEGF) formalism[41–44] combined with DFT, as implemented in the first principles quantum transport package Nanodcal.[41,45–47] In the NEGF-DFT self-consistent calculation, the wave functions and the other physical quantities are expanded with the linear combination of atomic orbital (LCAO) basis at the double-ζ polarization (DZP) level, the standard norm-conserving nonlocal pseudo-potentials[48] to describe the atomic core, and the generalized gradient approximation (GGA) with the Perdew–Burke–Ernzerhof (PBE) formulation applied for the exchange–correlation potential.[49] In the self consistent calculation, the first Brillouin zone of the electrodes is sampled using a 13 × 13 × 1 k space grid and the temperature is set at 100 K. In order to get accurate photoresponse values, the k space grid is set to be 50 × 1 × 1 during this part of the calculation. The NEGF-DFT self-consistency is

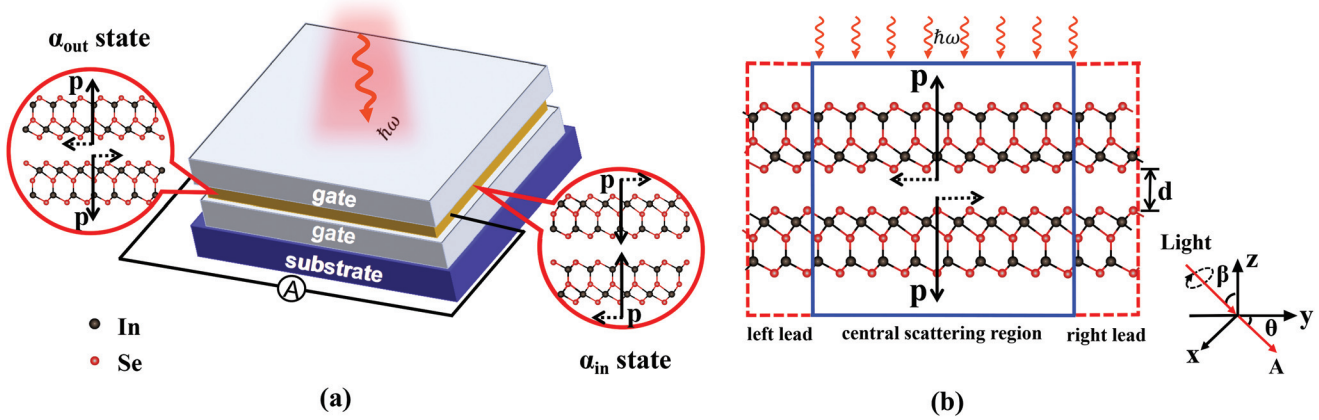

Fig. 1 (a) Schematic plot of the proposed opto-spintronic device based on anti-ferroelectric bilayer In_2Se_3. (b) The side view of the simulated anti-ferroelectric bilayer In_2Se_3 devices with polarization configuration α_{out}. The black arrows in each In_2Se_3 layer indicate the direction of ferroelectric polarization of the corresponding layer. There are three parts in the system, the left and right leads and the central scattering region where the light with photon energy $E_{ph} = \hbar\omega$ is shined. The black and red spheres represent In and Se atoms, respectively. Here A is the electromagnetic vector potential inside the x–y plane, θ denotes the polarization angle for the linearly polarized light and β is the corresponding photon incident angle with respect to the z direction.

deemed to be achieved when the monitored quantities such as every element of the Hamiltonian and density matrices differ less than 1×10^{-5} a.u. between the iteration steps. In a nutshell, the first principles of quantum transport calculations are conducted in two steps. Firstly, the two-probe device's Hamiltonian without considering electron–photon interaction is obtained using the NEGF-DFT self-consistently.[41] Secondly, the electron–photon interaction is perturbatively included as self-energy in terms of NEGF during the calculation of the photocurrent.[46]

For the two-probe device structure (see Fig. 1), the spin dependent photocurrent can be generated by shining linearly or circularly polarized light on the central scattering region which is indicated by the blue box. Moreover, the current flows from the electrode to the central region. In the following, we consider the photocurrent flowing in the left electrode of the two-probe structure. After obtaining the NEGF-DFT self-consistent device Hamiltonian, the spin dependent photocurrent $J_{\mathrm{L,s}}^{(\mathrm{ph})}$ is calculated in the first order Born approximation using the following formula,[46,50]

$$J_{\mathrm{L,s}}^{(\mathrm{ph})} = \frac{ie}{h}\int Tr\left\{\Gamma_{\mathrm{L}}\left[G_{\mathrm{ph}}^{<} + f_{\mathrm{L}}(\varepsilon)\left(G_{\mathrm{ph}}^{>} - G_{\mathrm{ph}}^{<}\right)\right]\right\}_{\mathrm{ss}} \mathrm{d}\varepsilon, \quad (1)$$

where L indicates the left electrode and s can be either the spin up or down component; $\Gamma_{\mathrm{L}} = i(\Sigma_{\mathrm{L}}^{\mathrm{r}} - \Sigma_{\mathrm{L}}^{\mathrm{a}})$ is the line width function of the left lead and $\Sigma_{\mathrm{L}}^{\mathrm{r}} = [\Sigma_{\mathrm{L}}^{\mathrm{a}}]^{\dagger}$ is the retarded self-energy due to the presence of the left lead; $f_{\mathrm{L}}(\varepsilon)$ is the Fermi–Dirac distribution function of the left lead; $G_{\mathrm{ph}}^{</>} = G_0^{\mathrm{r}}\Sigma_{\mathrm{ph}}^{</>}G_0^{\mathrm{a}}$ is the lesser/greater Green's function including electron–photon interaction,[51] where $\Sigma_{\mathrm{ph}}^{</>}$ is the self-energy due to the presence of the electron photon interaction. The information about the polarization of light is included in the self energy and can be characterized by a complex vector $\mathbf{e}$. For linearly polarized light, $\mathbf{e} = \cos\theta\ \mathbf{e_1} + \sin\theta\ \mathbf{e_2}$, where θ is the angle formed by the polarized direction with respect to the vector $\mathbf{e_1}$ (y axis as shown in Fig. 1(b)). In our numerical calculations, the vectors $\mathbf{e_1}$ and $\mathbf{e_2}$ are set along the y and x directions, respectively, *i.e.*, the light is incident along the -z direction with different incidence angles β, as shown in Fig. 1. For the elliptically polarized light, the polarization vector is defined as $\mathbf{e} = \cos\phi\ \mathbf{e_1} + i\sin\phi\ \mathbf{e_2}$. In particular, when $\phi = \pm 45°$, it represents the left/right circularly polarized light, respectively.

For simplicity, we introduce a spin dependent photocurrent response function to represent the normalized photocurrent,[50,51] *i.e.*,

$$R_{\mathrm{s}} = \frac{J_{\mathrm{L,s}}^{(\mathrm{ph})}}{eI_{\omega}}, \quad (2)$$

where $J_{\mathrm{L,s}}^{(\mathrm{ph})}$ is the spin dependent photocurrent defined in eqn (1); I_{ω} is the photon flux defined as the number of photons per unit time per unit area. Note that the photoresponse has dimension of area, a_0^2/photon where a_0 is the Bohr radius. In order to characterize the imbalance of the generated spin dependent photoresponse, the spin polarization (SP) is defined as,

$$\mathrm{SP}(\%) = \frac{\left||R_{\uparrow}| - |R_{\downarrow}|\right|}{|R_{\uparrow}| + |R_{\downarrow}|} \times 100, \quad (3)$$

where $R_{\uparrow/\downarrow}$ represents the spin up/down component of photoresponse of the left lead, respectively.

Furthermore, we introduce spin dependent relative photoresponse change ratio n_{s} to denote the relative changes of spin dependent photoresponse between α_{out} and α_{in} atomic structures,

$$n_{\mathrm{s}}(\%) = \frac{|R_{\mathrm{out,s}} - R_{\mathrm{in,s}}|}{|R_{\mathrm{out,s}}|} \times 100, \quad (4)$$

where $R_{\mathrm{out/in,s}}$ represents the photoresponse with spin component s in the $\alpha_{\mathrm{out,in}}$ structure, respectively.

As shown in Fig. 1(b), the two-terminal anti-ferroelectric bilayer In_2Se_3 based device can be divided into three regions: the central scattering region, and the left and right leads extending to the electron reservoirs to infinity. There are four unit cells with a total of 80 atoms in the central scattering region, about 28.44 Å. During the simulation, along the z direction, 10 Å vacuum layers are set at the top and bottom of the device to avoid the fake interaction between neighboring slabs. The linearly or circularly polarized light is shining on the central scattering region. In the following, we shall only consider the spin dependent photocurrent flowing into the left lead. θ and ϕ are the polarization angles of linearly polarized light and circularly polarized light, respectively. In numerical simulation, the x axis is along the transverse direction, the y axis is along the transport direction, and the z axis is perpendicular to the two dimensional system. According to the photogalvanic effect (PGE),[52–55] it is expected that spin dependent photocurrent can be generated under the irradiation of linearly or circularly polarized light without applying any external electric field. In the following section, we shall show that fully spin polarized photocurrent and pure spin current can also be produced in anti-ferroelectric bilayer In_2Se_3.

3. Results and discussion

To start with, we investigate bulk electronic structure properties of two anti-ferroelectric bilayer In_2Se_3 structures ($\alpha_{\mathrm{in/out}}$). The atomic structures are also shown in the inset figures in Fig. 2(a) and (b). It can be found that SOI plays a critically important role in determining the electronic properties of the In_2Se_3 structure, because the band structures for both atomic structures are different with and without SOI. The most significant difference is the indirect bandgap to direct bandgap transition feature when the SOI is included. By considering SOI, the bandgaps of the α_{out} and α_{in} structures are 0.69 eV and 0.63 eV, respectively. To further present the spin polarization of the bilayer In_2Se_3, we first determine a spin polarization vector $P = (P_x, P_y, P_z)$ from the Bloch state for specific energy E and then obtain the tilting angle Φ = arctan

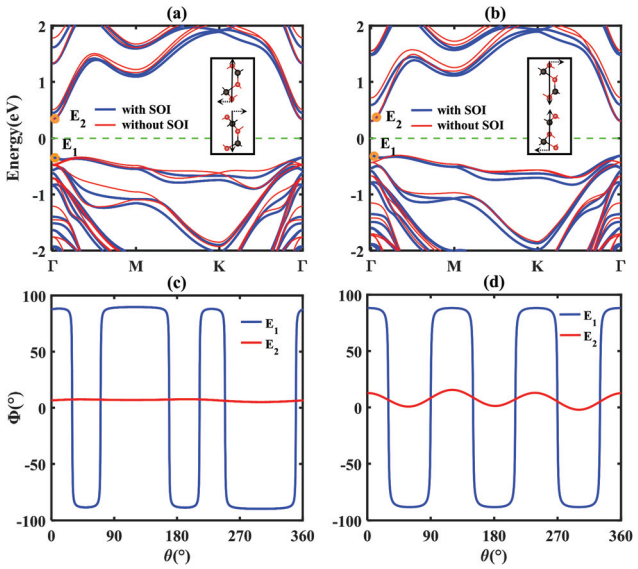

Fig. 2 (a, b) The band structure of two anti-ferroelectric bilayer In_2Se_3 systems with different polarization directions $\alpha_{out/in}$, respectively. The blue and red lines represent the band structure with or without SOI, respectively. The horizontal dashed green line represents the Fermi energy. (c, d) The corresponding tilting angle Φ *versus* polar angle θ with equal energy for the $\alpha_{out/in}$ structure, respectively. Here the blue and red lines correspond to the energies E_1 in the valence and E_2 in the conduction bands denoted as orange circles in panels (a, b). Note that E_1 = −0.343 eV and E_2 = 0.351 eV in (a, c) and E_1 = −0.316 eV, E_2 = 0.378 eV in (b, d).

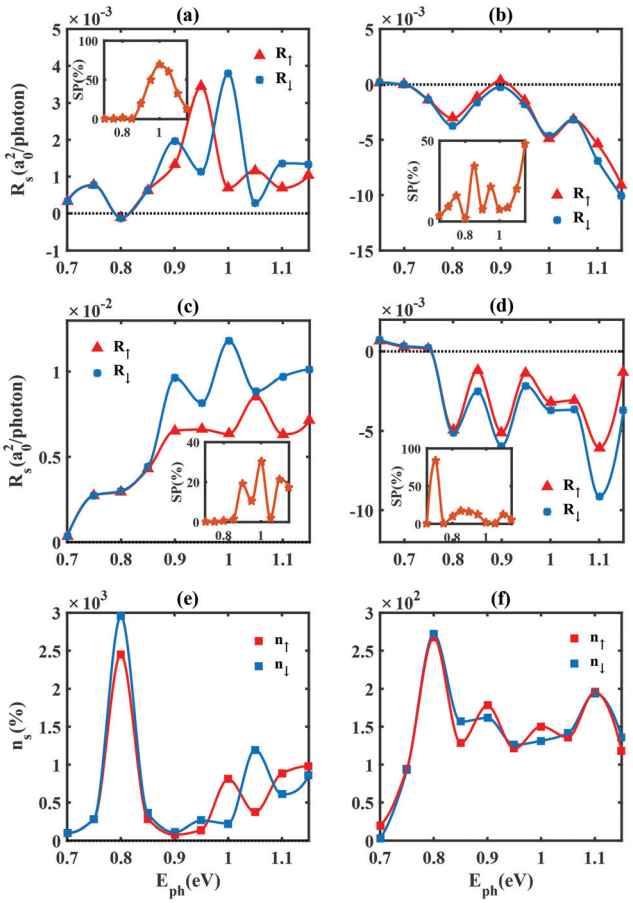

Fig. 3 The spin-dependent photoresponse *versus* the photon energy E_{ph} of the vertically incident linear polarized light. (a, c) The calculated spin dependent photoresponse for atomic structure α_{out} when the photon polarization is along the *y*-axis and *x*-axis, respectively. (b, d) The calculated spin dependent photoresponse for atomic structure α_{in} when the photon polarization is along the *y*-axis and *x*-axis, respectively. (e, f) The calculated spin dependent relative photoresponse change ratio n_s *versus* the photon energy when the photon polarization is along the *y*-axis and *x*-axis, respectively. Here, the red and blue lines represent the spin up and spin down components. The polarization angle θ is fixed θ = 0° in (a, b, e) and θ = 90° in (c, d, f). Note that the light in all these cases is incident vertically. The triangle, asterisk and square points are obtained from DFT calculations and the solid lines are fitted curves based on the calculated points.

$[P_z/(P_x^2 + P_y^2)^{1/2}]$ to characterize the spin texture.[56,57] In particular, the spin is perpendicular to the 2D plane when Φ = ±90°. Fig. 2(c and d) show Φ *versus* polar angle θ for the specific energies E_1 in the valence band and E_2 in the conduction band. Here angle θ is the polar angle in the (k_x,k_y) momentum plane, since the equal energy surface with energy E_i is a circle in two dimendion when it is around the Γ point. Clearly, Φ varies from −90° to 90° for energy E_1 while Φ is around zero for energy E_2 for both anti-ferroelectric bilayer In_2Se_3 structures. By comparing Fig. 2(c) and (d), we can find the spin polarization for both energies is quite different for the two anti-ferroelectric bilayer structures. This indicates that the spin polarization of photon excited electrons should be different even when the photon energy $E_{ph} = E_2 - E_1$ is fixed. This provides the possibility for us to regulate the spin dependent photocurrent *via* the PGE.

Having understood the bulk electronic properties and spin texture, we firstly analyze the spin-dependent photoresponse generated by the linearly polarized photogalvanic effect (LPGE) under vertical irradiation. The numerical results for the two different structures $\alpha_{out/in}$ are presented in Fig. 3. At first glance, we can clearly see that the generated photoresponse is in general spin-polarized in the studied photon energy range. It can be seen that due to the existence of spin–orbit coupling in the two structures with different polarization directions, the generated spin-up photocurrent and spin-down photocurrent are not equal, and they are spin-polarized. The corresponding spin polarizations are presented in the inset figures in Fig. 3 (a–d), from which we can know that the photoresponse spin polarization for both structures varies between 0% and 100% and can be tuned by changing the photon energy. It is interesting that the photocurrent may reverse its sign when the photon energy is changing, for example, the photocurrent is positive when E_{ph} is equal to 0.7 eV while it is negative when E_{ph} is equal to 0.8 eV, as shown in Fig. 3(d).[38] By further comparing Fig. 3(a/b) and (c/d), the generated photoresponses of the two atomic structures ($\alpha_{out/in}$) have large differences in the curve trend and magnitude for two spin components. As an example, the spin polarization of α_{out} is 60.7% while it is as small as 8.88% for α_{in} when the photon energy is equal to 1.05

eV. To demonstrate the relative difference, the spin dependent relative photoresponse change ratios n_s, defined in eqn (4) for two polarization angles, are quite large as presented in Fig. 3(e and f). These reveal that the proposed anti-ferroelectric In_2Se_3 can be used as an optical spintronic memory device, since two ferroelectric states can be switched into each other by an external gate voltage. Finally, it is found that the spin-dependent photoresponses for $\theta = 0°$ and $\theta = 90°$ have distinct features. Thus, the photoresponse sensitively depends on photon polarization θ. In the following, we shall investigate how the spin dependent photoresponse reacts with photon polarization angle θ.

Next, we study the effect of polarization angle θ of LPGE on the spin dependent photoresponse for two In_2Se_3 structures α_{in} and α_{out} by fixing the photon energy $E_{ph} = 0.8$ eV. The numerical results are presented in Fig. 4. It can be seen from Fig. 4(a and b) that the spin-dependent photoresponse can be greatly tuned by using the photon polarization angle θ. Correspondingly, the spin polarization for both structures can vary between 0% and 100%, as shown in Fig. 4(c). Note that the fully spin polarized current can be generated in both structures, while the pure spin current can be obtained in structure α_{out}. When the polarization angle θ is in the vicinity of 11.3° and 168.5°, the spin up and spin down photocurrent components in structure α_{out} have the same magnitude and opposite sign. Thus the spin polarization SP is 0% and hence the pure spin current is generated. For the fully spin polarized current, when the photon polarization angle θ is around 42°, the spin-down photocurrent of structure α_{out} is equal to 0. This results in fully spin polarized current with a spin-up photocurrent. When the photon polarization angle θ is around 138° only the spin down photocurrent exists, (see Fig. 4(a) and (c)). Similarly, there are several specific photon polarization angles to generate fully spin polarized (only spin up or down component) photocurrent in structure α_{in} (see Fig. 4(b) and (c)). Furthermore, the relative photoresponse change ratio n_s can also be largely adjusted by using the polarization angle θ, as shown in Fig. 4(d). A big difference between $n_\uparrow$ and $n_\downarrow$ is observed.

Finally, the spin dependent photoresponse and the corresponding spin polarization *versus* the incident angle β of the LPGE are studied and the results are presented in Fig. 5. Here the photon energy E_{ph} is also set as 0.8 eV and the polarization angle $\theta = 45°$. We found that the full spin polarized current can be obtained by adjusting the incident angle of linearly polarized light. For structure α_{out}, the incident angle β is near 73.7° to achieve fully spin polarized photocurrent with the spin down component, as shown in Fig. 5(a and c). In comparison, in structure α_{in}, the fully spin polarized photocurrent with the spin up component can be obtained when the incident angle is around 80.9°, as shown in Fig. 5(b and c). In addition, the relative photoresponse change ratio can also be tuned by the incident angle β as shown in Fig. 5(d) and the maximum value can be as large as 2×10^4. In the ESI,† the

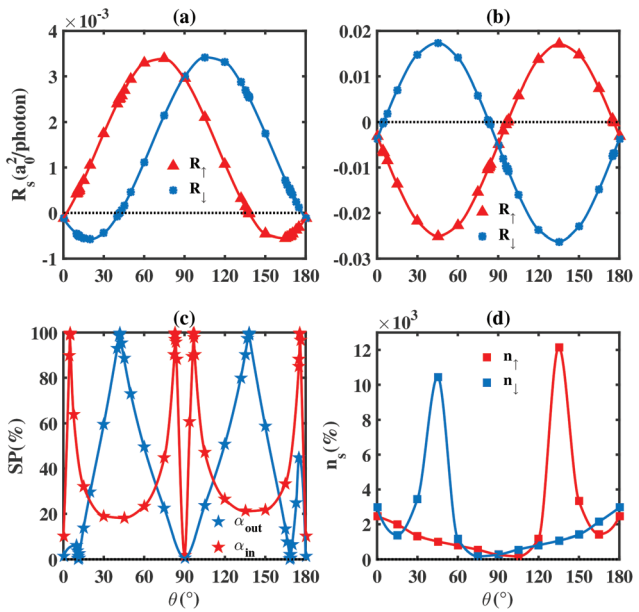

Fig. 4 (a, b) The spin dependent photoresponse *versus* the polarization angle θ of LPGE for two In_2Se_3 structures α_{out} and α_{in}, respectively. (c) The corresponding spin polarization of structures α_{out} and α_{in} *versus* the polarization angles θ. (d) spin dependent relative photoresponse change ratio *versus* the polarization angles θ. The photon energy E_{ph} is equal to 0.8 eV. The triangle, asterisk and square points are obtained from DFT calculations and the solid lines are the fitted curves based on the calculated points.

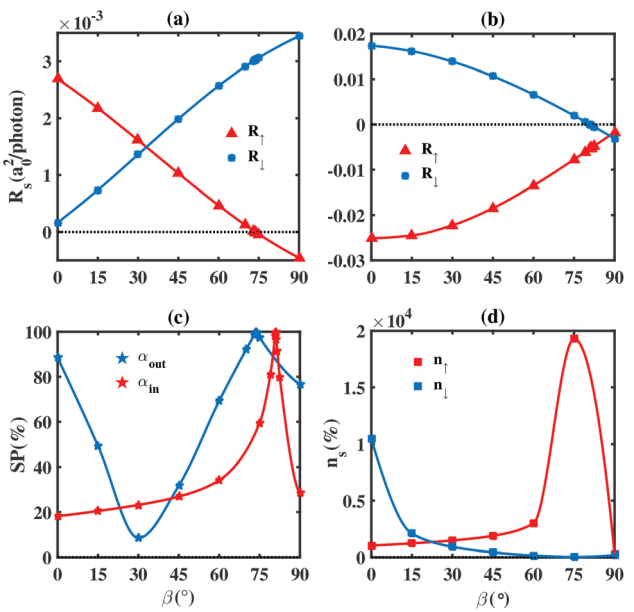

Fig. 5 (a, b) The photoresponse *versus* photon incident angle β for two In_2Se_3 structures α_{out} and α_{in}, respectively. (c) The corresponding spin polarization of structures α_{out} and α_{in} *versus* the photon incident angles β. (d) The spin dependent relative photoresponse change ratio *versus* the photon incident angles β. The photon energy E_{ph} is equal to 0.8 eV and its polarization angle is fixed at $\theta = 45°$. The triangle, asterisk and square points are obtained from DFT calculations and the solid lines are fitted curves based on the calculated points.

spin dependent photoresponse generated by the circularly PGE (CPGE) is also presented. It is found that the CPGE induced photoresponses are also spin polarized and can be tuned by the photon energies, photon polarization angles ϕ and incident angles β. More importantly, the relative spin photoresponse change ratios for both spin components are in the same order compared with that of the LPGE. Therefore, circularly polarized light can also be used to generate and tune the spin dependent photocurrent as linearly polarized light.

The experimental observation of our predicted effects relies on the ferroelectricity switch of two-dimensional material In_2Se_3 and spin dependent photocurrent detection. Actually, in the recent experimental work,[4] the ferroelectric domain (tens of μm^2) of thin layer In_2Se_3 (5 nm, around 4 layers) can be switched by an external electric field at room temperature. Thus, there is no restriction on the layer number of two-dimensional material In_2Se_3 for the ferroelectricity switch. To detect the generated spin dependent photocurrent, it is important to contact the ferromagnetic lead with the In_2Se_3 material, which can be achieved by the present experimental technique.[58] As an estimation, the generated photocurrent can reach 10^{-17} A (photoresponse R is in the order of 0.01) when the laser power is 1 $\mu W\ \mu m^{-2}$ (usually used in the experiment).

4. Conclusion

To summarize, we study the photogalvanic effect (PGE) induced spin dependent photoresponse in two anti-ferroelectric bilayer In_2Se_3 ($\alpha_{in/out}$) structures by atomic first-principles calculations. Due to the presence of strong SOI and lack of inversion symmetry for the anti-ferroelectric bilayer In_2Se_3 structures, the spin polarized photocurrent can be robustly generated *via* the LPGE or CPGE without the need for applying an external bias. By tuning the photon energies, polarization and incident angles, the fully spin polarized current can be produced for both structures. Furthermore, the pure spin current can also be obtained in the α_{out} structure by tuning the photon polarization angle, which is highly desired in spintronic applications. Most importantly, by switching the atomic structures between α_{in} and α_{out} states, the relative photoresponse change ratio n_s can reach the order of $\sim 10^4$. This indicates that our proposed anti-ferroelectric bilayer In_2Se_3 nanoscale device can be used as a non-volatile opto-spintronic device.

Conflicts of interest

There are no conflicts to declare.

Acknowledgements

We gratefully acknowledge the support from the National Natural Science Foundation of China (Grants No. 12074230, and 11974355), the National Key R&D Program of China under Grants No. 2017YFA0304203, 1331KSC, and the Shanxi Province 100-Plan Talent Program. This research was partially conducted using the High Performance Computer of Shanxi University.

References

1 N. Setter, D. Damjanovic, L. Eng, G. Fox, S. Gevorgian, S. Hong, A. Kingon, H. Kohlstedt, N. Park, G. Stephenson, I. Stolitchnov, A. Taganstev, D. Taylor, T. Yamada and S. Streiffer, *J. Appl. Phys.*, 2006, **100**, 051606.
2 L. Li, L. Xie and X. Pan, *Rep. Prog. Phys.*, 2019, **82**, 126502.
3 W. Zhou and A. Ariando, *Jpn. J. Appl. Phys.*, 2020, **59**, SI0802.
4 S. Wan, Y. Li, W. Li, X. Mao, W. Zhu and H. Zeng, *Nanoscale*, 2018, **10**, 14885–14892.
5 D. Damjanovic, *Rep. Prog. Phys.*, 1998, **61**, 1267.
6 H. Abdelkefi, H. Khemakhem, A. Simon and M. Maglione, *J. Appl. Phys.*, 2007, **102**, 114106.
7 V. M. Fridkin and B. Popov, *Sov. Phys. Usp.*, 1978, **21**, 981.
8 T. Sasaki and Y. Naka, *Opt. Rev.*, 2014, **21**, 99–109.
9 L. You, Y. Zhang, S. Zhou, A. Chaturvedi, S. A. Morris, F. Liu, L. Chang, D. Ichinose, H. Funakubo, W. Hu, T. Wu, Z. Liu, S. Dong and J. Wang, *Sci. Adv.*, 2019, **5**, eaav3780.
10 K. Mistewicz, M. Nowak and D. Stróż, *Nanomaterials*, 2019, **9**, 580.
11 H. Lu, A. Lipatov, S. Ryu, D. Kim, H. Lee, M. Y. Zhuravlev, C.-B. Eom, E. Y. Tsymbal, A. Sinitskii and A. Gruverman, *Nat. Commun.*, 2014, **5**, 1–7.
12 J. Hoffman, X. Pan, J. W. Reiner, F. J. Walker, J. Han, C. H. Ahn and T. Ma, *Adv. Mater.*, 2010, **22**, 2957–2961.
13 P. Hou, S. Xing, X. Liu, C. Chen, X. Zhong, J. Wang and X. Ouyang, *RSC Adv.*, 2019, **9**, 30565–30569.
14 C. Cui, W.-J. Hu, X. Yan, C. Addiego, W. Gao, Y. Wang, Z. Wang, L. Li, Y. Cheng, P. Li, X. Zhang, H. N. Alshareef, T. Wu, W. Zhu, X. Pan and L.-J. Li, *Nano Lett.*, 2018, **18**, 1253–1258.
15 S. Wan, Y. Li, W. Li, X. Mao, C. Wang, C. Chen, J. Dong, A. Nie, J. Xiang, Z. Liu, W. Zhu and H. Zeng, *Adv. Funct. Mater.*, 2019, **29**, 1808606.
16 L. Kang, P. Jiang, N. Cao, H. Hao, X. Zheng, L. Zhang and Z. Zeng, *Nanoscale*, 2019, **11**, 16837–16843.
17 L. Kang, P. Jiang, H. Hao, Y. Zhou, X. Zheng, L. Zhang and Z. Zeng, *Phys. Rev. B*, 2020, **101**, 014105.
18 J. Xiao, H. Zhu, Y. Wang, W. Feng, Y. Hu, A. Dasgupta, Y. Han, Y. Wang, D. A. Muller, L. W. Martin, P. Hu and X. Zhang, *Phys. Rev. Lett.*, 2018, **120**, 227601.
19 A. V. Bune, V. M. Fridkin, S. Ducharme, L. M. Blinov, S. P. Palto, A. V. Sorokin, S. Yudin and A. Zlatkin, *Nature*, 1998, **391**, 874–877.
20 C. Cui, F. Xue, W.-J. Hu and L.-J. Li, *npj 2D Mater. Appl.*, 2018, **2**, 1–14.
21 S. Shen, C. Liu, Y. Ma, B. Huang and Y. Dai, *Nanoscale*, 2019, **11**, 11864–11871.
22 Z. Guan, H. Hu, X. Shen, P. Xiang, N. Zhong, J. Chu and C. Duan, *Adv. Electron. Mater.*, 2020, **6**, 1900818.

23 L. Dai, *J. Semicond.*, 2019, **40**, 060402–060402.
24 W. Ding, J. Zhu, Z. Wang, Y. Gao, D. Xiao, Y. Gu, Z. Zhang and W. Zhu, *Nat. Commun.*, 2017, **8**, 14956.
25 C. Zheng, L. Yu, L. Zhu, J. L. Collins, D. Kim, Y. Lou, C. Xu, M. Li, Z. Wei, Y. Zhang, M. T. Edmonds, S. Li, J. Seide, Y. Zhu, J. Z. Liu, W.-X. Tang and M. S. Fuhre, *Sci. Adv.*, 2018, **4**, eaar7720.
26 F. Xue, W. Hu, K.-C. Lee, L.-S. Lu, J. Zhang, H.-L. Tang, A. Han, W.-T. Hsu, S. Tu, W.-H. Chang, C.-H. Lien, J.-H. He, Z. Zhang, L.-J. Li and X. Zhang, *Adv. Funct. Mater.*, 2018, **28**, 1803738.
27 J. Quereda, R. Biele, G. Rubio-Bollinger, N. Agraït, R. D'Agosta and A. Castellanos-Gomez, *Adv. Opt. Mater.*, 2016, **4**, 1939–1943.
28 J. O. Island, S. I. Blanter, M. Buscema, H. S. van der Zant and A. Castellanos-Gomez, *Nano Lett.*, 2015, **15**, 7853–7858.
29 Z. Zhang, J. Yang, F. Mei and G. Shen, *Front. Optoelectron.*, 2018, **11**, 245–255.
30 B. Tang, L. Hou, M. Sun, F. Lv, J. Liao, W. Ji and Q. Chen, *Nanoscale*, 2019, **11**, 12817–12828.
31 P. Hou, S. Xing, X. Liu, C. Chen, X. Zhong, J. Wang and X. Ouyang, *RSC Adv.*, 2019, **9**, 30565–30569.
32 R. Wang, T. Wang, Y. Zhou, Y. Wu, X. Zhang, X. He, H. Peng, J. Zhao and X. Qiu, *2D Mater.*, 2019, **6**, 035034.
33 Z. Zheng, P. Chen, J. Lu, J. Yao, Y. Zhao, M. Zhang, M. Hao and J. Li, *Sci. China Mater.*, 2020, **63**, 1560–1569.
34 L. Debbichi, O. Eriksson and S. Lebègue, *J. Phys. Chem. Lett.*, 2015, **6**, 3098–3103.
35 Y. Xie, M. Chen, Z. Wu, Y. Hu, Y. Wang, J. Wang and H. Guo, *Phys. Rev. Appl.*, 2018, **10**, 034005.
36 H. Xu, H. Wang, J. Zhou and J. Li, arXiv e-prints, 2020, arXiv:2006.16945.
37 R.-C. Xiao, D.-F. Shao, Y.-H. Li and H. Jiang, arXiv e-prints, 2020, arXiv:2009.02748.
38 J. Chen, L. Zhang, L. Zhang, X. Zheng, L. Xiao, S. Jia and J. Wang, *Phys. Chem. Chem. Phys.*, 2018, **20**, 26744–26751.
39 X. Tao, P. Jiang, H. Hao, X. Zheng, L. Zhang and Z. Zeng, *Phys. Rev. B*, 2020, **102**, 081402.
40 G. Kresse and J. Furthmüller, *Phys. Rev. B: Condens. Matter Mater. Phys.*, 1996, **54**, 11169–11186.
41 J. Taylor, H. Guo and J. Wang, *Phys. Rev. B: Condens. Matter Mater. Phys.*, 2001, **63**, 245407.
42 M. Zhai, X. Wang, P. Vasilopoulos, Y. Liu, Y. Dong, L. Zhou, Y. Jiang and W. You, *Nanoscale*, 2014, **6**, 11121–11129.
43 A. Saraiva-Souza, M. Smeu, L. Zhang, M. A. Ratner and H. Guo, *J. Phys. Chem. C*, 2016, **120**, 4605–4611.
44 L. Zhang, Z. Yu, L. Zhang, X. Zheng, L. Xiao, S. Jia and J. Wang, *J. Mater. Chem. C*, 2018, **6**, 2460–2466.
45 For details of the NanoDcal quantum transport package, see, http://www.nanoacademic.ca.
46 L. Zhang, K. Gong, J. Chen, L. Liu, Y. Zhu, D. Xiao and H. Guo, *Phys. Rev. B: Condens. Matter Mater. Phys.*, 2014, **90**, 195428.
47 D. Waldron, P. Haney, B. Larade, A. MacDonald and H. Guo, *Phys. Rev. Lett.*, 2006, **96**, 166804.
48 L. Kleinman and D. Bylander, *Phys. Rev. Lett.*, 1982, **48**, 1425.
49 J. P. Perdew, K. Burke and M. Ernzerhof, *Phys. Rev. Lett.*, 1996, **77**, 3865.
50 J. Chen, Y. Hu and H. Guo, *Phys. Rev. B: Condens. Matter Mater. Phys.*, 2012, **85**, 155441.
51 L. E. Henrickson, *J. Appl. Phys.*, 2002, **91**, 6273–6281.
52 E. Ivchenko and G. Pikus, *JETP Lett.*, 1978, **27**, 640–643.
53 Y. Xie, L. Zhang, Y. Zhu, L. Liu and H. Guo, *Nanotechnology*, 2015, **26**, 455202.
54 S. Ganichev, E. Ivchenko, V. Bel'kov, S. Tarasenko, M. Sollinger, D. Weiss, W. Wegscheider and W. Prettl, *Nature*, 2002, **417**, 153–156.
55 C. Jiang, V. Shalygin, V. Y. Panevin, S. N. Danilov, M. Glazov, R. Yakimova, S. Lara-Avila, S. Kubatkin and S. Ganichev, *Phys. Rev. B: Condens. Matter Mater. Phys.*, 2011, **84**, 125429.
56 Y. Zhao, Y. Hu, L. Liu, Y. Zhu and H. Guo, *Nano Lett.*, 2011, **11**, 2088–2091.
57 K. Gong, L. Zhang, D. Liu, L. Liu, Y. Zhu, Y. Zhao and H. Guo, *Nanotechnology*, 2014, **25**, 435201.
58 E. C. Ahn, *npj 2D Mater. Appl.*, 2020, **4**, 1–14.